Population Shift between the Open and Closed States Changes the Water Permeability of an Aquaporin Z Mutant

Lin Xin,[†‡§] Claus Hélix-Nielsen,[¶‖] Haibin Su,[**] Jaume Torres,[‡] Chuyang Tang,[†§] Rong Wang,[†§] Anthony Gordon Fane,[†§] and Yuguang Mu[‡*]

[†]School of Civil and Environmental Engineering, [‡]School of Biological Sciences, and [§]Singapore Membrane Technology Centre, Nanyang Technological University, Singapore; [¶]DTU Physics, Technical University of Denmark, Lyngby, Denmark; [‖]Aquaporin A/S, Copenhagen, Denmark; and **School of Material Sciences, Nanyang Technological University, Singapore

ABSTRACT Aquaporins are tetrameric transmembrane channels permeable to water and other small solutes. Wild-type (WT) and mutant Aquaporin Z (AqpZ) have been widely studied and multiple factors have been found to affect their water permeability. In this study, molecular dynamics simulations have been performed for the tetrameric AqpZ F43W/H174G/T183F mutant. It displayed ~10% average water permeability compared to WT AqpZ, which had been attributed to the increased channel lumen hydrophobicity. Our simulations, however, show a ring stacking between W43 and F183 acting as a secondary steric gate in the triple mutant with R189 as the primary steric gate in both mutant and WT AqpZ. The double gates (R189 and W43-F183) result in a high population of the closed conformation in the mutant. Occasionally an open state, with diffusive water permeability very close to that of WT AqpZ, was observed. Taken together, our results show that the double-gate mechanism is sufficient to explain the reduced water permeability in the mutant without invoking effects arising from increased hydrophobicity of the channel lumen. Our findings provide insights into how aquaporin-mediated water transport can be modulated and may further point to how aquaporin function can be optimized for biomimetic membrane applications.

INTRODUCTION

Aquaporins (AQPs) are members of the major intrinsic protein family (1). They are integral membrane proteins functioning as homotetramers with each monomer forming a channel through the lipid bilayer. Aquaporins are found throughout the kingdom of life where their main function is associated with selective permeation of water and other small solutes across biological membranes (2,3). According to their substrate selectivity aquaporins can be divided into two subfamilies, the orthodox aquaporins that are permeable to water only and the aquaglyceroporins that conduct both water and small solutes such as glycerol and metalloids (4,5). Besides being objects for fundamental research AQPs are increasingly attracting attention as building blocks in biomimetic membrane developments (6,7) where the development of strategies for large scale biomimetic membranes may lead to separation devices based on the unique water selectivity properties of AQPs (8–10). It therefore becomes important to elucidate the structural mechanism(s) behind AQP permeation and gating.

Currently, atomic resolution x-ray structures of 21 AQPs (including mutants) are available (11). An exclusive list of AQPs with high resolution structure can be found in the website: http://blanco.biomol.uci.edu/mpstruc/listAll/list#id_TRANSMEMBRANE_PROTEINS_ALPHAHELICAL, which is maintained by Stephen White lab. A comparison of these structures reveals a common structural theme with six transmembrane helices connected by five loops. For each aquaporin monomer, a single aqueous channel lumen is surrounded by the six helices with two half-helices pointing into the channel and toward the lipid bilayer midplane. An ar/R (aromatic/arginine) selectivity filter (SF) created by a cluster of amino acids located around 8 Å away from the midplane toward the extracellular side constitutes the mechanism by which the AQP is able to selectively bind water molecules allowing them to permeate while preventing other molecules from entering the channel lumen (12).

Considering the high overall structural similarity, the water permeability and substrate selectivity are likely to be modulated mainly by the channel lining residues. Early mutagenesis work has shown that substitution of a tyrosine and a tryptophan by a proline and a leucine, respectively, on positions P4P5 of an insect AQP (AQPcic) abolished the water transfer but allowed glycerol passage (13). Mutations to alanine of residues at the SF region in AQP1 drastically increased SF size, and increased permeability to glycerol, urea, ammonia, and protons, but had nearly no effect on water permeability compared to wild-type (WT) AQP1 (14). It has also been shown that hydrogen bond donor/acceptors H180 or R195 in AQP1 are dispensable for water sequestration and AQP1 water permeability is independent on the polarity at the ar/R SF region (14).

On the basis of these observations, it is difficult to rationalize which factors may affect AQP permeability. Mutagenesis studies may seem the obvious way to identify residues affecting water selectivity and permeability. However, point mutations may introduce multiple effects: they may change the local polarity (14,15), change the local structure and channel size (14), change the water orientation inside the

Submitted December 5, 2011, and accepted for publication May 30, 2012.

*Correspondence: ygmu@ntu.edu.sg

Editor: Jose Faraldo-Gomez.

0006-3495/12/07/0212/7 $2.00

http://dx.doi.org/10.1016/j.bpj.2012.05.049

channel (12), change the channel size, and may even change the overall stability of the AQP functional tetramer (16). Thus, in general it is a nontrivial task to identify specific factors affecting AQP water selectivity and permeability.

With high resolution AQP protein structures now available, molecular dynamics (MD) simulations constitute a valuable tool for studying mechanisms underlying water permeability, substrate selectivity, and channel gating. In principle MD allows for resolving the experimentally inaccessible ps to ns dynamics of the protein and water movements. Indeed, many MD simulation studies have been performed to investigate AQP protein gating (17), proton/ion exclusion mechanism (18,19), as well as water permeation (20–22). Thus, the presence of open-closed dual states in aquaporin Z (AqpZ) has been directly related to the side-chain conformation of residue R189 located in the SF region (20,23). The extremely high conservation of R189 attests to its functional role. However, there is no experimental evidence of the open-closed mechanism apart from the two AqpZ forms captured by x-ray crystal structures presumably representing the open and closed states (24). It is also very difficult to compare the calculated single channel permeability (e.g., obtained from MD simulations) with values obtained from experimental measurements because the latter represent average equilibrium permeabilities of large AQP ensembles consisting of both open and closed channels.

In a recent experiment directed toward enhancing AQP permeability to glycerol three mutations at the channel lining residues F43, H174, and T183 were introduced in AqpZ. The resulting mutant F43W/H174G/T183F was found to retain only 10% water permeability compared to the WT AqpZ (15). The high resolution crystal structures of the F43W/H174G/T183F mutant showed no change in pore size at the SF region relative to WT AqpZ. Therefore, these mutations were suggested to reduce water permeability by reducing the polarity around the SF. However, the crystal structure also showed that the side chain of R189 is in a down conformation, which corresponds to the WT AqpZ closed state identified in simulations (20) and in the WT crystal structure (24). We have shown that in the closed state of WT AqpZ channel, the steric effect alone can shut down the water flow (20). This may suggest that in the F43W/H174G/T183F mutant the equilibrium between the open and closed states may also be regulated by R189.

We therefore undertook MD simulations to reveal water permeation dynamics through the mutant F43W/H174G/T183F AqpZ. Our results show that i), the mutant AqpZ channel may switch between open and closed states—just like the WT AqpZ; ii), the polar to nonpolar mutations do not change the single channel water permeability in the open state relative to the WT AqpZ; iii), the water permeability is regulated by the R189 side-chain conformational change; iv), a ring stacking between W43 and F183 side chains provides an additional gate to regulate water transportation. The result shows that the collective side chain-side chain dynamics of R189, W44, and F183 in the mutant results in a redistribution of the open and closed states. The induced high population of the closed state corresponds to the experimentally observed low water permeability of F43W/H174G/T183F.

MATERIALS AND METHODS

Detailed information of the system setup and simulation protocols can be found in the Supporting Material.

RESULTS AND DISCUSSION

The F43W/H174G/T183F mutant reveals open and closed states

To characterize the water permeability of the F43W/H174G/T183F mutant, a total of eight tetrameric MD simulations have been performed starting from the recently published crystal structure PDB 3NK5 (15). In this structure, the side chain of R189 is in a down conformation with its guanidinium group pointing into the channel thus blocking water transport. This is reflected in all 32 mutant monomer trajectories where initially only very few permeation events were observed corresponding to the water permeation rate k_0 being almost zero.

However, as the simulations progressed in time, significant water permeation was observed in three monomer simulations. Continuous water permeation through these three channels was observed for periods of 17 ns, 80 ns, and 20 ns, respectively. The water permeation rate k_0 during this open state of the three monomer channels were 0.5/ns, 0.4/ns, and 0.95/ns and are comparable to k_0 obtained from simulations of the WT AqpZ open conformation (20). Thus, the F43W/H174G/T183F mutant exhibits open and closed state behavior and water permeability just like the WT AqpZ.

R189 side-chain conformation and channel permeability

Our previous study showed that the open-closed states of WT AqpZ can be directly related to the side-chain conformation of R189 (the R gate) (20). The osmotic permeability of the channel and the water permeation rate are both directly related to the distance (D_{oh}) between the nitrogen atom (NH1) on the side chain of R189 and the backbone carbonyl oxygen atom of A117. In the crystal structure, D_{oh} of the open and the closed channel is 0.263 and 0.466 nm, respectively. We therefore used D_{oh} to characterize the open and closed states for the F43W/H174G/T183F mutant.

Fig. 1 shows the results from two tetramer simulations (Fig. 1, *A* and *C* and *B* and *D*, respectively), where the simulations were started with different random initial velocities but otherwise under identical conditions. Of the eight

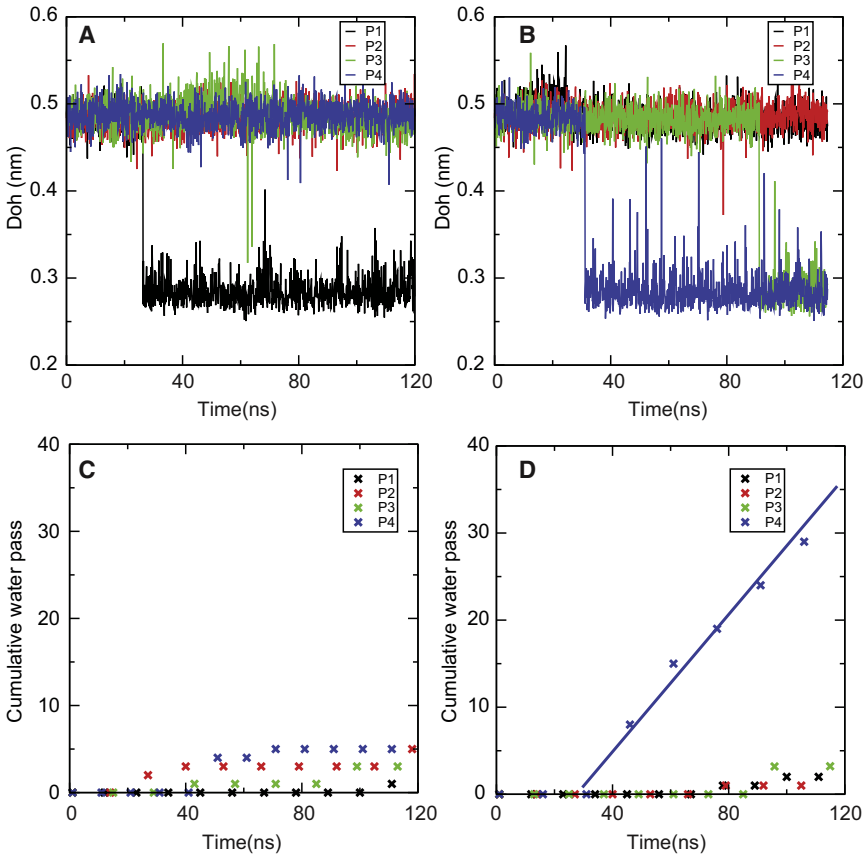

FIGURE 1 Distance between Arg-189NH1 and A117O, D_{oh}, as a function of time (*A* and *B*). Cumulative water passing events as a function of simulation time (*C* and *D*). *A* and *C* are from trajectory 1, *B* and *D* are from trajectory 2. P1-4 denotes the single channel in the tetramer.

monomer simulations only monomer channel P4 in simulation 2 becomes open after 34 ns and remains open throughout the simulation with constant water permeation (see Fig. 1 *D*). The D_{oh} of P4 decreases abruptly from a value around 0.48 nm to a value around 0.28 nm at 32 ns (see Fig. 1 *B*). The observed decrease in D_{oh} corresponds to D_{oh} in the WT AqpZ closed-to-open transition. It is clear that, with no decrease of D_{oh}, the mutant monomer channels remain closed as observed in P2, P3, and P4 in simulation 1 and P1 and P2 in simulation 2. Furthermore, in all simulations, when a channel is in the open state, the values of D_{oh} are always low (around 0.28 nm). However, in the mutant some monomer channels still remain closed even when D_{oh} is close to 0.28 nm, such as P1 in simulation 1 after 28 ns and P2 in simulation 2 after 92 ns. This indicates that a small D_{oh} is a necessary but not a sufficient condition for the mutant channel to assume an open state. We therefore investigated what other factors could affect the open-to-closed transition of the mutant monomer channels.

Ring stacking of W43 and F183 can block the mutant channel water transport

To investigate the structural changes leading to closing of the mutant channel with R189 side chain in the open conformation (D_{oh} around 0.28 nm) we compared hydrogen bond formation occurrences in the open and closed mutant channels (data not shown). The largest differences were observed in a region close to the SF where the mutated residues T183F and F43W are located. In the crystal structure the distance between the toluene ring of F183 and the methylindole ring of W43 is <0.4 nm, which indicates a close ring stacking (25). Because these two residues locate around the narrowest region inside the channel, we speculated that their side-chain conformational change may affect the channel permeation ability.

To resolve the correlation among the distance between the centers of mass of the W43 methylindole ring and F183 toluene ring (D_{WF}), D_{oh} and water permeation, we constructed the two-dimensional distribution functions of D_{WF} and D_{oh} compiled from all simulations and this is shown in Fig. 2. The distributions were obtained for both the open and the closed states, where the two states were classified by the presence or absence of permeating water molecules, respectively. We define a permeating water molecule as a water molecule passing through the channel from the extracellular side to the cytoplasmic side or vice versa during the simulation time.

The analysis reveals clear differences in the distribution of both D_{oh} and D_{WF} between the closed and open states of the mutant channel. In the closed state, most D_{oh} and D_{WF} values are located around 0.5 and 0.6 nm, respectively,

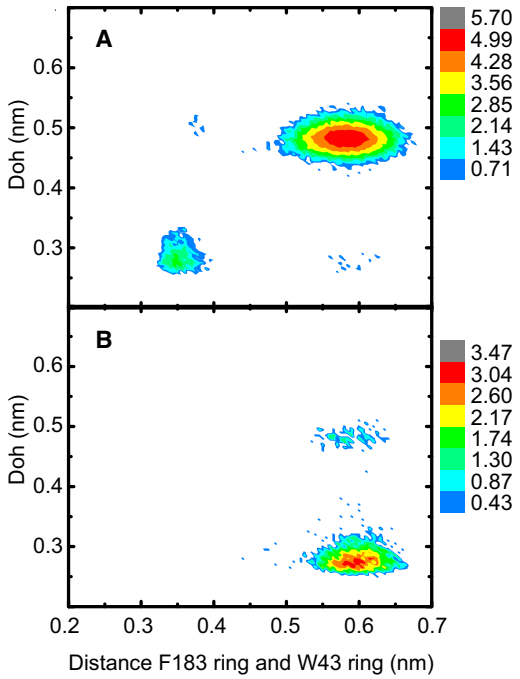

FIGURE 2 Occurrence distribution of D_{oh} and the distance between the rings from W43 and F183 side chains, D_{WF}, for the closed (*A*) and open state (*B*) based on all simulation data. The color scale is based on the logarithm of the occurrence counts.

which reflect a conformation with the R gate closed and the rings of W43 and F183 in an unstacked conformation. Interestingly, there are also considerable contributions from a second set of D_{oh} and D_{WF} values centered around 0.27 and 0.35 nm, respectively, corresponding to a conformation where the R gate is open and that the rings from W43 and F183 are stacked. In the open state most D_{oh} and D_{WF} values are centered around 0.27 and 0.6 nm, respectively. This corresponds to an open R gate and an unstacked ring conformation of W43/F183.

It is thus likely that the ring stacking between the F183 and W43 side chains serves as a second gate (the FW gate) that can modulate water transport in the mutant monomer channels. When a single monomer is open (i.e., shows water transport), it has a small D_{oh}, and there is no ring stacking between F183 and W43 side chains and both gates are open, see columns 2, 3, and 6 in Fig. S1. When there is ring stacking, even if D_{oh} is small (R gate open), the channel remains closed because the FW gate is closed. Therefore, we propose that the F43W/H174G/T183F mutant has a gating mechanism mediated by F183-W34 interactions. The time course of the stacking formation as revealed by D_{WF} can be found in the Supporting Material (Fig. S2).

The F183-W43 ring stacking depends on R189 side-chain conformation

Interestingly, in most simulations the ring stacking between F183 and W43 side chain is only observed when D_{oh} is small. To investigate this correlation further we analyzed the cumulative distributions of D_{WF} for the two situations where R189 is in the open or closed conformation (see Fig. 3). Clearly, when the R189 side chain is in the closed conformation, there is no ring stacking (i.e., negligible occurrences of D_{WF} below 0.4 nm). When the R189 side chain is in the open conformation, the frequency of the ring stacking occurrency increases significantly. Assuming that stacking requires $D_{WF} < 0.42$ nm, the ratio between the stacking and nonstacking states is 48:52 when the R gate is open. A snapshot of the closed FW gate is shown in Fig. 4 *A*; the stacking of the two rings blocks water permeation. In the open state, gates (R and FW), are open and water molecules can pass in a single file pattern, see Fig. 4 *B*.

Without external forces, a water molecule can diffuse through an open channel by jumping between available hydrogen bond sites in the channel. A network of hydrogen bond acceptors for water inside the channel is formed and this is shown in Fig. 4 (*lower panel*) for the mutant channel. A node represents a hydrogen bond acceptor. The lines connecting the nodes indicate the occurrence of water jumping between the hydrogen bond acceptor sites as observed in the simulations. The translocation between site S184O and N182O through acceptor sites at R189, W43, and F183 is the crucial step, because that region corresponds to the minimum pore radius in the open channel. It is clear that for a closed channel, the space between R189, W43, and F183 side chains is so small that water molecules are sterically excluded from the region, which completely inhibits the migration of water between S184O and N182O.

Factors affecting water permeability

Here and in our previous study (20), we have calculated the diffusive and osmotic permeability of AQPs. However, it is

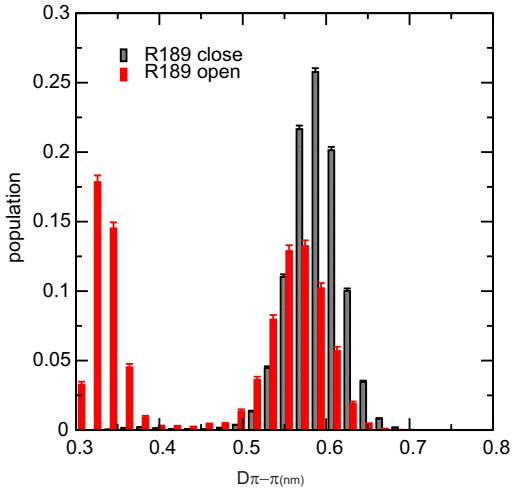

FIGURE 3 Distribution of distance between the rings of W43 and F183 side chain, D_{WF}, under the condition of open (*red bars*) and closed (*gray bars*) R189-gate based on all simulation data.

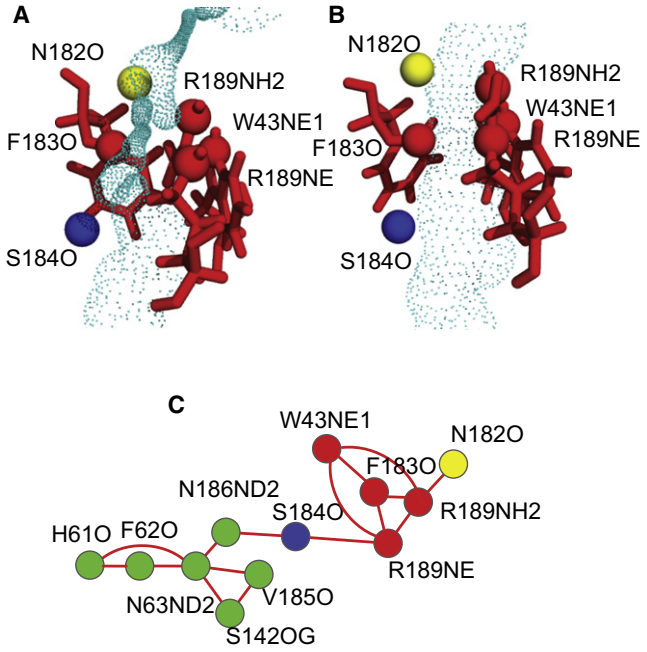

FIGURE 4 Side-chain conformation and HOLE representation of the channel around the SF region for a WF-gate closed configuration (*A*) and an open water channel (*B*). Water permeation pathway through the SF region (*C*). Water molecules hopping between the hydrogen bond acceptors in the SF region.

difficult to compare the calculations directly with experimental values such as the permeability obtained from stopped-flow osmotic measurements of AQP-containing vesicles. The reason is that a stopped-flow experiment measures the permeability provided by the ensemble of functional AQPs incorporated into the vesicular membrane. Furthermore, it is extremely difficult to test the existence of the open and closed states related to the side-chain conformation of R189, because the experimental (ensemble-based) measurements are on a timescale of seconds, whereas the transition between open and closed states are in the ns range. Thus, the ensemble averaged permeability measured by experiments cannot directly confirm the existence of dual permeation states. On the other hand, simulations can readily provide the fraction of time that the gate is open and the permeability of water in the open state; together, these two measures provide an estimate of channel permeability that can be compared to experimental values (see below).

When comparing the water permeation rate for the open channel of the mutant with that of the WT, we note that there is no significant difference. The effective lumen hydrophobicity increase induced by the triple mutation does not seem to affect the water permeability of the open channel. As suggested previously, steric effect seems to be more prominent in changing AqpZ single channel permeability by simply opening up or closing the channel lumen.

The lumen radius value distributions for the narrowest (SF) part of the channel in the open and closed states provide information about the closing mechanism (see Fig. 5, which is based on all simulation data). When the channel is open, the minimum lumen radius is distributed around a mean value of 0.1 nm, which is similar to that of the WT AqpZ. Thus, the triple mutation does not affect the water passage in the open state. In the closed state, however, the minimum lumen radius decreases to 0.05 nm, this completely closes the channel. This is consistent with the closed R or FW gate providing steric hindrance for water permeation.

Because the open states for both the mutant and the WT have the same water permeability, it is very likely that the experimentally measured difference in overall permeability between the mutant and the WT may be due to a difference in populations of open states. In this study, the total population of the open channel can be estimated from the ratio between the sum of observed time intervals in which water permeation occurs and the total time simulated for all monomers. Thus, we obtain a ratio of $((17\ \text{ns} + 80\ \text{ns} + 20\ \text{ns})/(6 \times 4 \times 50\ \text{ns} + 2 \times 4 \times 120\ \text{ns})) = 0.054$. In our previous study (20), we used the potential of mean force and calculated the population of the open channel state for the WT to be 0.45, which is 8.3 times higher than that of the mutant calculated here. The calculated water permeability of mutant and WT channels can be compared to the measured rate constant of liposome shrinkage from stopped-flow experiments where the rate constant for shrinking in the presence of the mutant proteins is 12.3 s^{-1}, whereas that in the presence of the WT proteins is 102 s^{-1} (15). The

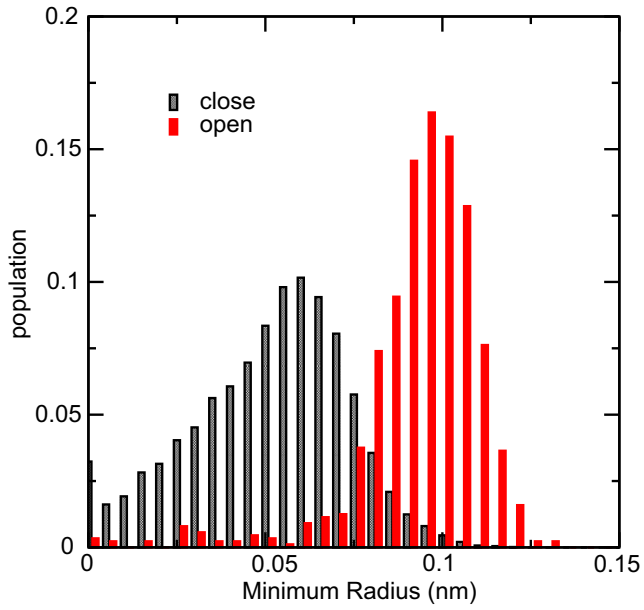

FIGURE 5 Distribution of the minimum radius value of water channel under the condition of open (*red bars*) and closed (*gray bars*) channel based on all simulation data.

experimental rate constant ratio is thus 8.5—close to our calculated water permeability ratio of 8.3.

Obviously, we should not put too much emphasis on the good numerical fit between the theoretical and experimental WT/mutant water permeability ratios, because the estimate is based on a small number of opening transitions observed in the simulations. Furthermore, it is difficult to ensure full convergence for such a large simulation system. Nevertheless, given the observation that the water permeability of the open channel is not affected by the mutations, it strongly suggests that for the mutant AQP, the double R189 and W43/F183 gate, and not the associated hydrophobicity change in the channel lumen environment, represents the underlying mechanism for the low water permeability of the mutant.

Experimental support for this notion can be found in the observation that changing polarity in AQP1 around the ar/R constriction SF site through individual or joint replacement of His-180 and Arg-195 by alanine and valine residues, respectively (AQP1-H180A, AQP1-R195V, and AQP1-H180A R195V), does not affect water permeability (14). In this case the increased channel size compensates for the effect of increased hydrophobicity of the SF region. On the other hand, a polar environment does not necessarily enhance water transportation in microscopic channels: a point charge inside a hydrophobic channel can even completely abolish water flow (26). Also for the AqpZ L170C mutant, when a positively charged mercury ion resides in the channel, water molecules hydrate the ion and the hydrated ion blocks the channel (27). This is consistent with the notion of water-pore interactions complemented by steric effects as the key determinants underlying the selectivity mechanism in AQPs and aquaglyceroporins (28). Aquaglyceroporins have minimum lumen radius of around 0.35 nm to allow the passage of glycerol and other uncharged solutes while water permeation is diminished (29), which was explained by the increased hydrophobicity (22). However, it does not apply for PfAQP, an aquaglyceroporin from the malarial parasite *Plasmodium falciparum* (30,31). PfAQP can transport both water and glycerol at high rates—yet it is highly homologous to *Escherichia coli* GlpF, which is hardly permeated by water. The triple mutant studied here cannot convert a water-only transporter, AQPZ, into a glycerol transporter, but instead reduce water permeability due to the invoking of a second gate. In this regard, PfAQP turns out to be a successful mutant of GlpF by nature. Based on our current study and the observation that the conserved arginine in the selectivity filter is constrained by three hydrogen bonds in PfAQP similar to other water-selective aquaporins (31), a similar R-gate and related population shift favoring the open state may also apply to PfAQP. Thus, we conclude that water permeability arises from a complex interplay between channel lumen shape, local hydrophobicity, overall stability perturbations of the protein induced by changes in e.g., the membrane environment (32,33), and population shifts between metastable states governed by correlated side-chain dynamics (e.g., the double gating observed here).

CONCLUSION

In this study, the open and closed states of AQP F43W/H174G/T183F triple mutant are found to be not only related to the side-chain conformation of R189 but also to the ring stacking between W43 and F183 side chains. The latter interaction provides a second gate capable of modulating the water flow through the mutant channel. We suggest that the dual gates lead to an increased population of the closed state explaining the low water permeability measured for the F43W/H174G/T183F mutant. This does not exclude other mechanisms for modulation of water permeability, such as constraints arising from channel lumen shape, local hydrophobicity, and overall stability perturbations of the protein.

SUPPORTING MATERIAL

Materials and methods, two figures, and references (34–41) are available at http://www.biophysj.org/biophysj/supplemental/S0006-3495(12)00631-5.

The support of the Environment Water Industry Programme Office under the National Research Foundation of Singapore (grant MEWR MEWR651/06/169), MOE Tier I research project RG23/11, and suggestions of anonymous reviewers are gratefully acknowledged.

REFERENCES

1. Borgnia, M., S. Nielsen, …, P. Agre. 1999. Cellular and molecular biology of the aquaporin water channels. *Annu. Rev. Biochem.* 68:425–458.
2. King, L. S., D. Kozono, and P. Agre. 2004. From structure to disease: the evolving tale of aquaporin biology. *Nat. Rev. Mol. Cell Biol.* 5:687–698.
3. Murata, K., K. Mitsuoka, …, Y. Fujiyoshi. 2000. Structural determinants of water permeation through aquaporin-1. *Nature.* 407:599–605.
4. Carbrey, J. M., and P. Agre. 2009. Discovery of the aquaporins and development of the field. *Handb. Exp. Pharmacol.* 3–28.
5. Nielsen, C. H. 2010. Major intrinsic proteins in biomimetic membranes. *Adv. Exp. Med. Biol.* 679:127–142.
6. Kumar, M., M. Grzelakowski, …, W. Meier. 2007. Highly permeable polymeric membranes based on the incorporation of the functional water channel protein Aquaporin Z. *Proc. Natl. Acad. Sci. USA.* 104:20719–20724.
7. Nielsen, C. H. 2009. Biomimetic membranes for sensor and separation applications. *Anal. Bioanal. Chem.* 395:697–718.
8. Hansen, J. S., M. Perry, …, C. H. Nielsen. 2009. Large scale biomimetic membrane arrays. *Anal. Bioanal. Chem.* 395:719–727.
9. Vogel, J., M. E. Perry, …, O. Geschke. 2009. Support structure for biomimetic applications. *J. Micromech. Microeng.* 19:025026.
10. González-Pérez, A., K. B. Stibius, …, O. G. Mouritsen. 2009. Biomimetic triblock copolymer membrane arrays: a stable template for functional membrane proteins. *Langmuir.* 25:10447–10450.
11. Törnroth-Horsefield, S., K. Hedfalk, …, R. Neutze. 2010. Structural insights into eukaryotic aquaporin regulation. *FEBS Lett.* 584: 2580–2588.

12. Tajkhorshid, E., P. Nollert, …, K. Schulten. 2002. Control of the selectivity of the aquaporin water channel family by global orientational tuning. *Science.* 296:525–530.

13. Lagrée, V., A. Froger, …, I. Pellerin. 1999. Switch from an aquaporin to a glycerol channel by two amino acids substitution. *J. Biol. Chem.* 274:6817–6819.

14. Beitz, E., B. Wu, …, T. Zeuthen. 2006. Point mutations in the aromatic/arginine region in aquaporin 1 allow passage of urea, glycerol, ammonia, and protons. *Proc. Natl. Acad. Sci. USA.* 103:269–274.

15. Savage, D. F., J. D. O'Connell, 3rd, …, R. M. Stroud. 2010. Structural context shapes the aquaporin selectivity filter. *Proc. Natl. Acad. Sci. USA.* 107:17164–17169.

16. Borgnia, M. J., D. Kozono, …, P. Agre. 1999. Functional reconstitution and characterization of AqpZ, the *E. coli* water channel protein. *J. Mol. Biol.* 291:1169–1179.

17. Tournaire-Roux, C., M. Sutka, …, C. Maurel. 2003. Cytosolic pH regulates root water transport during anoxic stress through gating of aquaporins. *Nature.* 425:393–397.

18. Phongphanphanee, S., N. Yoshida, and F. Hirata. 2008. On the proton exclusion of aquaporins: a statistical mechanics study. *J. Am. Chem. Soc.* 130:1540–1541.

19. de Groot, B. L., and H. Grubmüller. 2005. The dynamics and energetics of water permeation and proton exclusion in aquaporins. *Curr. Opin. Struct. Biol.* 15:176–183.

20. Xin, L., H. Su, …, Y. Mu. 2011. Water permeation dynamics of AqpZ: a tale of two states. *Biochim. Biophys. Acta.* 1808:1581–1586.

21. Jensen, M. O., E. Tajkhorshid, and K. Schulten. 2003. Electrostatic tuning of permeation and selectivity in aquaporin water channels. *Biophys. J.* 85:2884–2899.

22. de Groot, B. L., and H. Grubmüller. 2001. Water permeation across biological membranes: mechanism and dynamics of aquaporin-1 and GlpF. *Science.* 294:2353–2357.

23. Hub, J. S., C. Aponte-Santamaría, …, B. L. de Groot. 2010. Voltage-regulated water flux through aquaporin channels in silico. *Biophys. J.* 99:L97–L99.

24. Savage, D. F., P. F. Egea, …, R. M. Stroud. 2003. Architecture and selectivity in aquaporins: 2.5 a x-ray structure of aquaporin Z. *PLoS Biol.* 1:E72.

25. Chelli, R., F. L. Gervasio, …, V. Schettino. 2002. Stacking and T-shape competition in aromatic-aromatic amino acid interactions. *J. Am. Chem. Soc.* 124:6133–6143.

26. Li, J., X. Gong, …, R. Zhou. 2007. Electrostatic gating of a nanometer water channel. *Proc. Natl. Acad. Sci. USA.* 104:3687–3692.

27. Zhang, Y. B., Y. B. Cui, and L. Y. Chen. 2012. Mercury inhibits the L170C mutant of aquaporin Z by making waters clog the water channel. *Biophys. Chem.* 160:69–74.

28. Hub, J. S., and B. L. de Groot. 2008. Mechanism of selectivity in aquaporins and aquaglyceroporins. *Proc. Natl. Acad. Sci. USA.* 105: 1198–1203.

29. Fu, D. X., A. Libson, …, R. M. Stroud. 2000. Structure of a glycerol-conducting channel and the basis for its selectivity. *Science.* 290: 481–486.

30. Beitz, E., S. Pavlovic-Djuranovic, …, J. E. Schultz. 2004. Molecular dissection of water and glycerol permeability of the aquaglyceroporin from *Plasmodium falciparum* by mutational analysis. *Proc. Natl. Acad. Sci. USA.* 101:1153–1158.

31. Newby, Z. E. R., J. O'Connell, 3rd, …, R. M. Stroud. 2008. Crystal structure of the aquaglyceroporin PfAQP from the malarial parasite *Plasmodium falciparum. Nat. Struct. Mol. Biol.* 15:619–625.

32. Andersen, O. S., C. Nielsen, …, R. E. Koeppe, II. 1998. Gramicidin channels as molecular force transducers in lipid bilayers. *Biol. Skr. Dan. Vid. Selsk.* 49:75–82.

33. Nielsen, C., M. Goulian, and O. S. Andersen. 1998. Energetics of inclusion-induced bilayer deformations. *Biophys. J.* 74:1966–1983.

34. Jorgensen, W. L., J. Chandrasekhar, …, M. L. Klein. 1983. Comparison of simple potential functions for simulating liquid water. *J. Chem. Phys.* 79:926–935.

35. Van Der Spoel, D., E. Lindahl, …, H. J. Berendsen. 2005. GROMACS: fast, flexible, and free. *J. Comput. Chem.* 26:1701–1718.

36. MacKerell, Jr., A. D., N. Banavali, and N. Foloppe. 2000-2001. Development and current status of the CHARMM force field for nucleic acids. *Biopolymers.* 56:257–265.

37. Lindahl, E., P. Bjelkmar, …, B. Hess. 2010. Implementation of the CHARMM force field in GROMACS: analysis of protein stability effects from correction maps, virtual interaction sites, and water models. *J. Chem. Theory Comput.* 6:459–466.

38. Bussi, G., D. Donadio, and M. Parrinello. 2007. Canonical sampling through velocity rescaling. *J. Chem. Phys.* 126:014101.

39. Berendsen, H. J. C., J. P. M. Postma, …, J. R. Haak. 1984. Molecular-dynamics with coupling to external bath. *J. Chem. Phys.* 81: 3684–3690.

40. Darden, T., L. Perera, …, L. Pedersen. 1999. New tricks for modelers from the crystallography toolkit: the particle mesh Ewald algorithm and its use in nucleic acid simulations. *Structure.* 7:R55–R60.

41. Smart, O. S., J. M. Goodfellow, and B. A. Wallace. 1993. The pore dimensions of gramicidin A. *Biophys. J.* 65:2455–2460.